

# Development of smart transducer with embedded sensor for automatic process control of ultrasonic wire bonding

Siu Wing Or† and Helen Lai Wa Chan‡

Department of Applied Physics and Materials Research Centre, The Hong Kong Polytechnic University,  
Hung Hom, Kowloon, Hong Kong

Peter Chou Kee Liu‡†

ASM Assembly Automation Ltd., 4/F., Watson Centre, 16 Kung Yip Street,  
Kwai Chung, N.T., Hong Kong

(Received October 23, 2003, Accepted July 27, 2004)

**Abstract.** A ring-shaped lead zirconate titanate (PZT) piezoceramic sensor has been integrated with the Langevin-type piezoceramic driver of an ultrasonic wire-bonding transducer to form a *smart* transducer for in-situ measurement of three essential bonding parameters: namely, impact force, ultrasonic amplitude and bond time. This sensor has an inner diameter, an outer diameter and a thickness of 12.7 mm, 5.1 mm and 0.6 mm, respectively. It has a specifically designed electrode pattern on the two major surfaces perpendicular to its thickness along which polarization is induced. The process-test results have indicated that the sensor not only is sensitive to excessive impact forces exerted on the devices to be bonded but also can track changes in the ultrasonic amplitude proficiently during bonding. Good correlation between the sensor outputs and the bond quality has been established. This *smart* transducer has good potential to be used in automatic process-control systems for ultrasonic wire bonding.

**Keywords:** lead zirconate titanate (PZT); piezoceramic, ring sensor; *smart* transducer; ultrasonic wire bonder; ultrasonic wire bonding; automatic process control.

---

## 1. Introduction

Ultrasonic wire bonding is an important technology in the microelectronics packaging industry to provide electrical interconnections between the bond pads on integrated circuit (IC) chips and the leads on substrates (Fig. 1). It is based on the proper transmittal of ultrasonic vibration energy under pressure to plasticize the metallic fine wires (typically aluminum or gold wires) for forming metallurgical bonds by means of an ultrasonic transducer mounted on an ultrasonic wire bonder (Fig. 2a). As a key component of the wire bonder (Fig. 2b), the transducer basically consists of a Langevin-type

---

†Lecturer, Corresponding Author, E-mail: [apswor@polyu.edu.hk](mailto:apswor@polyu.edu.hk)

‡Chair Professor, E-mail: [apahlcha@polyu.edu.hk](mailto:apahlcha@polyu.edu.hk)

‡†Chief Technical Officer, E-mail: [peter.liu@asmpt.com](mailto:peter.liu@asmpt.com)

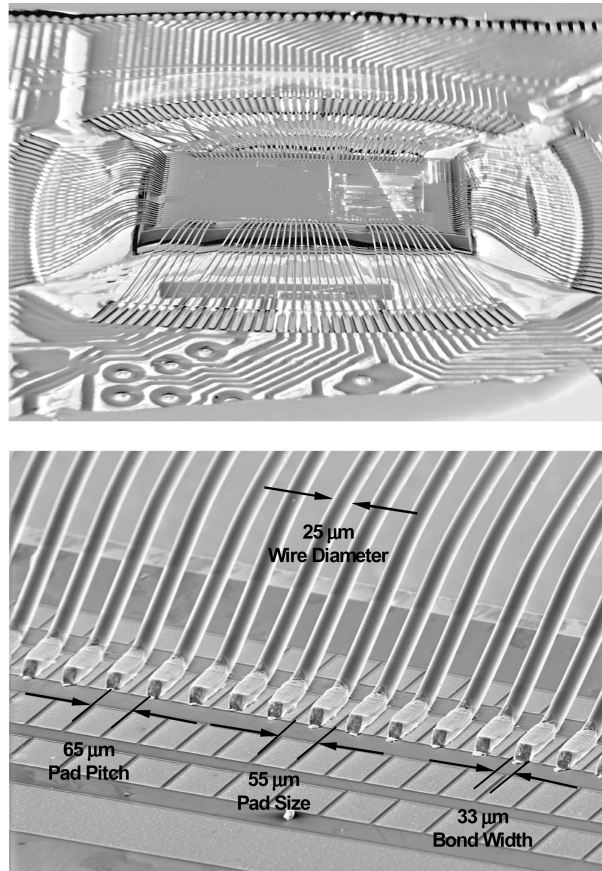


Fig. 1 Ultrasonic wire bonding of aluminum wires on an ASM standard chip-on-board (COB) test device

piezoelectric driver (a stack of piezoelectric rings sandwiched between two metal plates under a mechanical pressure exerted by a central prestress screw) for converting electrical driving signals from an ultrasonic signal generator into ultrasonic vibrations (typically at  $\sim 60$  kHz), an ultrasonic horn for amplifying the vibrations from the driver with the maximum amplitude at its smaller end, a bonding tool for holding the bond wire while coupling the vibrations at/to its tip, and a barrel for mounting the whole transducer onto the wire bonder so that the predetermined bond force can be applied, together with the ultrasonic vibrations, to the wire-pad/lead interfaces via the tip of the tool. In practice, an ultrasonic wire-bonding process can be described by the following four sequential steps (Charles 1989, Harman 1997):

1. The transducer with its tool (threaded with bond wire) is positioned over the first bonding site of the device.
2. The transducer is lowered to apply a predetermined bond force to press the wire against the bonding surface.
3. A burst of ultrasonic power is applied via the transducer to the bond zone for a preset bond time.
4. The transducer is lifted up and positioned at the second bonding site for completing a bonded wire.

As microelectronic devices are shrinking in size and increasing in complexity at a very rapid rate, automatic wire bonders need to move to higher degree of automation with higher production rate ( $>20$  wires/second) in order to catch up with the productivity and competitiveness. Besides, a poor bond can

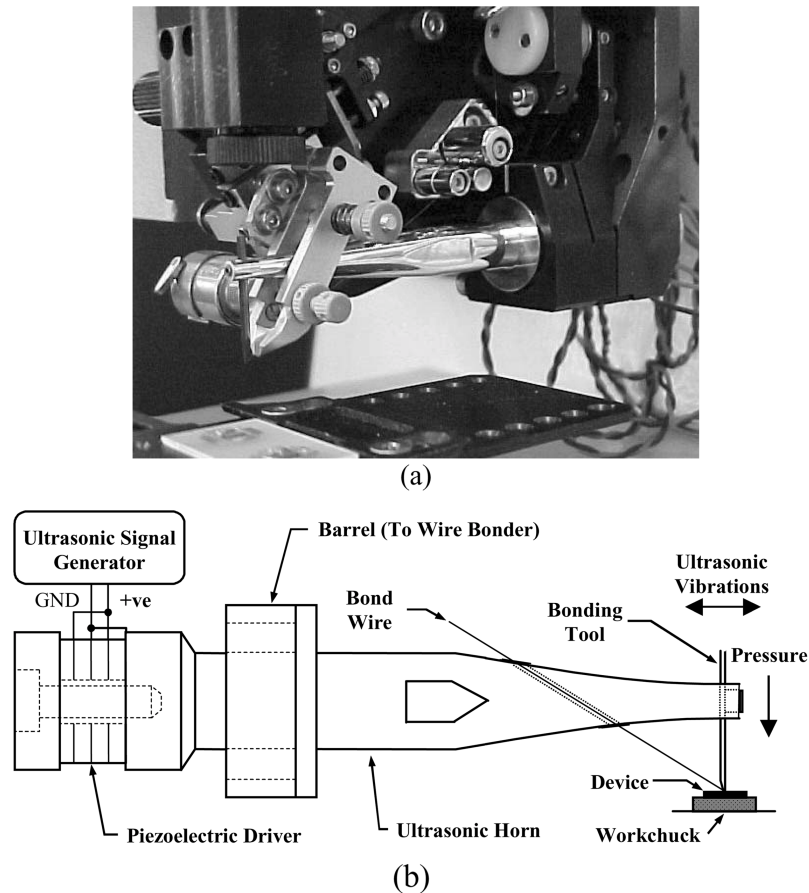


Fig. 2 An ultrasonic wire-bonding transducer and its wire bonder. (a) Photograph, (b) Schematic diagram

directly result in a total failure of a device. Therefore, it is vital to develop a reliable in-process monitoring system to improve the reliability and quality of bonding (Rodwell and Worrall 1985, Harman 1997). Recent research suggested that changes in the mechanical impedance of the bond zone during bond formation not only cause changes in the vibration characteristics of an ultrasonic wire-bonding transducer but also induce vibrations to the workchuck underneath the device to be bonded (Or, *et al.* 1998a, Hu, *et al.* 2003). The vibration information is different from bond to bond depending on whether the tool tip is free, fixed or damped in some way. For process control purpose, the most important bonding parameters are the impact force, the ultrasonic vibration amplitude and the bond time. By attaching piezoceramic sensors either to the surface of the transducer horn (Pufall 1993, Or, *et al.* 1998b) or to the workchuck (Chan, *et al.* 1999), the bond quality can be monitored in-situ by observing the temporal profile of the ultrasonic vibration amplitude. However, two crucial problems have significantly impeded their use. The first is no significant detection of the impact force and a separate sensor is required for impact force measurement (Chan, *et al.* 1999), while the second is difficulties in locating all sensors on a transducer. We have developed a single polyvinylidene fluoride (PVDF) piezopolymer sensor to measure the three bonding parameters by incorporating it in the driver-horn interface of a transducer so that the sensor/transducer (the primary version of the current *smart*

transducer) can readily be transported from one wire bonder to another (Chan, *et al.* 2001a, Chiu, *et al.* 2003). Nevertheless, the detection sensitivity is not high enough in general due to the sensor-driver collocation problem.

In this article, we report the use of a ring-shaped lead zirconate titanate (PZT) piezoceramic sensor to obtain an advanced measurement of both the impact force and ultrasonic amplitude as a function of bond time. This ring sensor, which has the same outer and inner diameters as the PZT piezoceramic ring stack of the transducer driver and a specifically designed electrode pattern, is installed as an integral part of the driver in a 62 kHz transducer, thereby forming a *smart* transducer possessing the attractive functionality of sensing-while-actuation with a high degree of sensor-driver collocation.

## 2. The smart transducer

### 2.1. Structure and operating principle

Fig. 3(a) shows the prototype of a 62 kHz *smart* transducer for use in ultrasonic wedge bonding and the solid model is illustrated in Fig. 3(b). The transducer has a length of 106.5 mm, corresponding to 1.5 longitudinal wavelengths at 62 kHz. It consists of a *smart* driver, an ultrasonic horn, a bonding tool (in form of a wedge) and a barrel.

Referring to Fig. 3(b), the *smart* driver (25.3 mm long) basically is a combination of a traditional Langevin-type piezoelectric driver (Fig. 2) and a piezoelectric sensor. It functions as a half-wave, longitudinal, mass-spring-mass, linear vibrator to convert the electrical energy generated by an ultrasonic signal generator (not shown) into longitudinal vibrations at 62 kHz; at the same time, the embedded sensor can measure three crucial bonding parameters, including the impact force, ultrasonic amplitude and bond time, due to the changes in the bond zone during bonding. The piezoelectric sensor selected for transducer fabrication is a moderately hard PZT ring sensor (ASM8 from ASM Assembly Automation Ltd., Hong Kong) with an outer diameter of 12.7 mm, an inner diameter of 5.1 mm and a thickness of 0.6 mm. This material possesses the distinct advantages of high electromechanical coupling factor ( $k_{33}=0.680$ ), low dissipation factor ( $\tan \delta_e = 0.35\%$ ), high stress handling capability (Young's modulus,  $Y_{33}^E = 63$  GPa) and high thermal stability (Curie temperature,  $T_c=320$  °C). The upper segment of the sensor is coated with silver electrode on the two major surfaces perpendicular to its thickness, and polarization is induced along the thickness direction using these patterned electrode surfaces. This specific pattern of electrode has been proven to give optimized outputs in a previous study (Chu, *et al.* 2003). The sensor is installed in between the driving piezoelectric stack and back plate of the Langevin driver. This location is capable of providing an optimal sensitivity for bond quality monitoring. Details on the selection of sensor location will be reported in Section 3.2. The driving piezoelectric stack employed comprises four ASM8 PZT rings connected electrically in parallel and mechanically in series to increase the output mechanical displacement and to reduce the input electrical impedance (Neppiras 1973). These rings have the outer and inner diameters the same as the ring sensor but with an increased thickness of 2.4 mm. The front and back plates are made of stainless steel. Five pieces of 0.04 mm thick, ring-shaped copper electrodes are interposed between the rings of the driving stack, sensor and back plate to provide electrical interconnection and external-connection with an ultrasonic signal generator (not shown). To enable the attachment of external electrical leads on the sensor while isolating the sensor signals from the driving signals, a 0.05 mm thick, ring-shaped polyimide film, which has a sputtered gold electrode with a pattern similar to the ring sensor on one side, is inserted

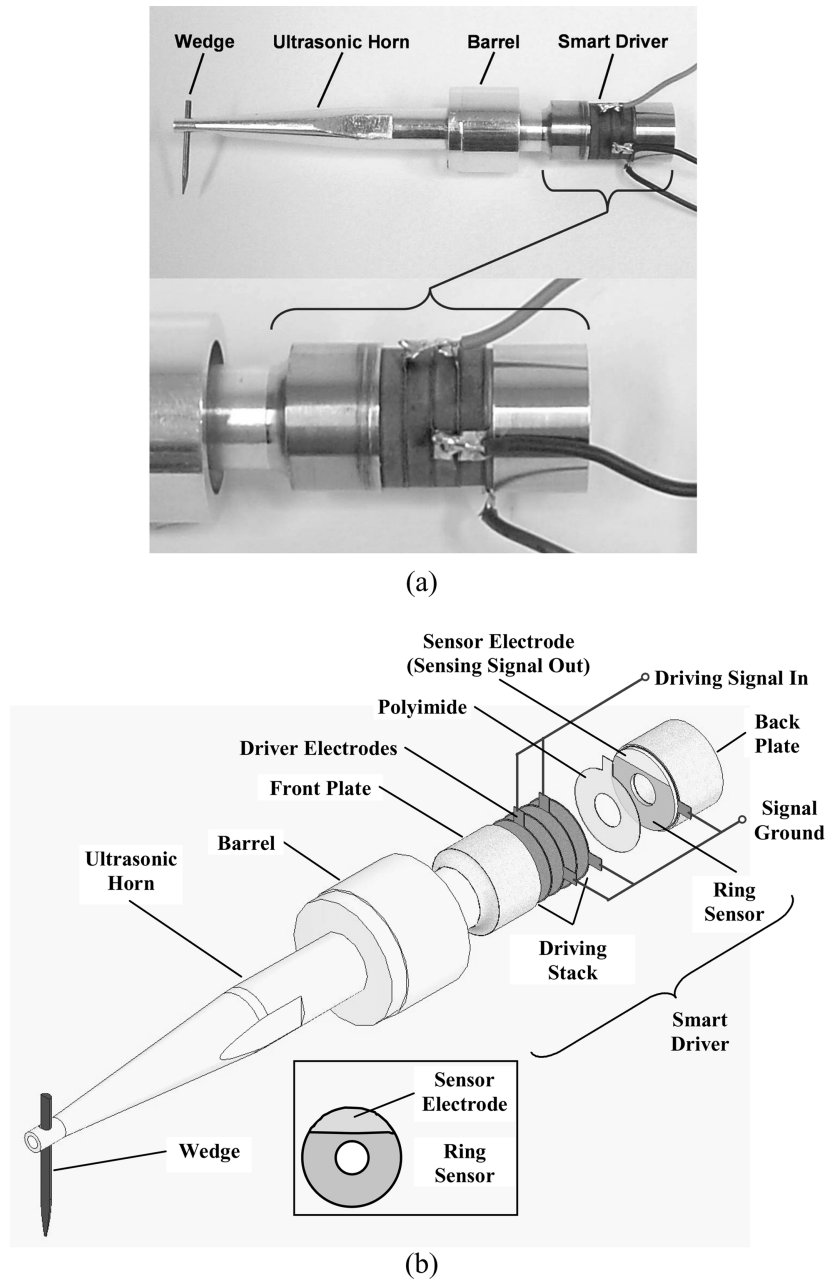


Fig. 3 The *smart* ultrasonic wire-bonding transducer. (a) Prototype, (b) Solid model

between the driving stack and the sensor such that this sputtered electrode is in contact with the patterned ring electrode. Great care has to be taken to ensure the alignment of these electrode patterns.

The ultrasonic horn, which is made of aluminium alloy, is formed by two half-wave sectional horns. The section next to the driver is a cylindrical horn (40.7 mm long). The second section is a two-section horn (40.5 mm long) having a cylindrical horn attached at the small end of a conical horn. The

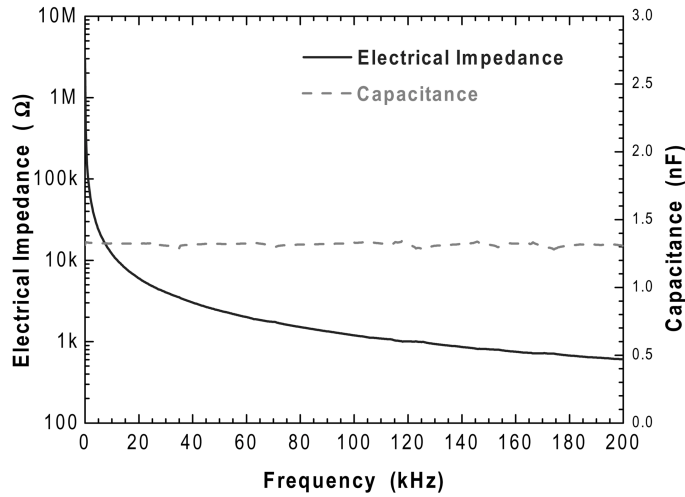


Fig. 4 Electrical impedance and capacitance spectra of the ring sensor in the *smart* transducer

ultrasonic horn is capable of amplifying three folds the longitudinal displacement output from the *smart* driver at its smaller end for coupling to a tungsten carbide wedge of 21 mm long and of providing a displacement node on the cylindrical section for fixing the barrel. This nodal point mounting can effectively minimize loss of energy and hence degradation of bonding performance (Frederick 1975, Graff 1975).

## 2.2. Sensor performance

After the transducer fabrication, the spectral response of the sensor was measured by an impedance analyzer (Agilent 4294A). Fig. 4 shows the electrical impedance and its capacitance spectra of the sensor. It is clear that the sensor behaves as a capacitor (capacitance=1.3 nF) with no prominent resonances for frequencies up to 200 kHz. This suggests that the sensor has a sufficiently flat frequency response for detecting impact forces and ultrasonic signatures.

## 2.3. Transducer performance

The electrical resonance characteristics of the *smart* transducer were also measured using the impedance analyzer and the results are plotted in Fig. 5. The strongest minimum impedance resonance is observed at 62.4 kHz, which is the resonance frequency of the transducer and the ultrasonic signal generator (not shown) should be tuned to lock at this point in order to maintain the transducer at resonance during bonding.

Fig. 6 shows the corresponding vibration mode shape of the transducer computed using a finite element modal analysis (ANSYS 7.0 from ANSYS, Inc., Canonsburg, PA). The computed resonance frequency is 64.1 kHz, which is in good agreement with the measured value of 62.4 kHz in Fig. 5 (agreed to 2.7%), thus confirming the validity of the transducer design and fabrication. It should be noted that the longitudinal-flexural motion as illustrated in Fig. 6 is the most desirable motion in ultrasonic wedge bonding. From a physical standpoint, a pure longitudinal expansion and contraction of the length of the transducer driver and horn causes the tip of the wedge to move back and forth axially

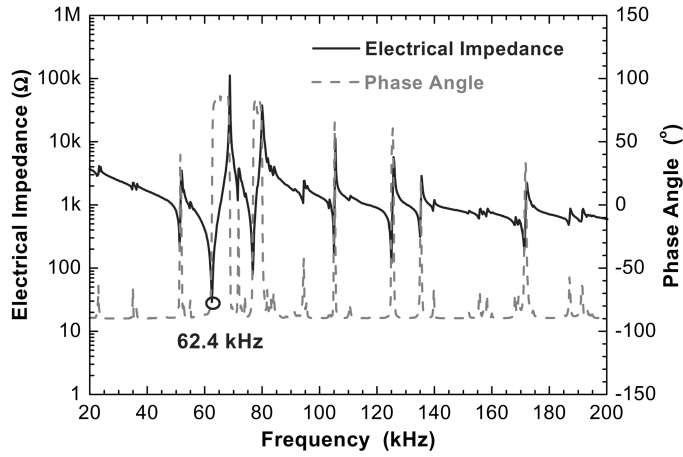


Fig. 5 Electrical impedance spectrum of the *smart* transducer

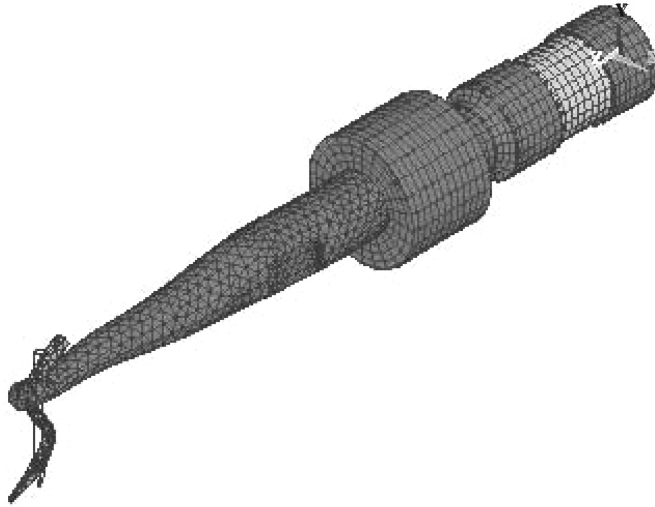


Fig. 6 Computed vibration mode shape of the *smart* transducer at 64.1 kHz

(Z-axis) for facilitating the largest flexural displacement. As this motion is essentially in line with the wire to be bonded which gives rise to the shape of the resulting wire bonds (Fig. 1), longitudinal-flexural mode is the desired operating mode in the *smart* transducer.

To reinforce our previous findings, the vibration distribution along the wedge was measured, in steps of 0.25 mm, using a laser Doppler vibrometer (Polytec OFV-303) connected to an oscilloscope (HP 54504). The displacement values are calculated from the measured velocity amplitudes using

$$u = \frac{v}{\omega} \quad (1)$$

where  $u$  is the displacement amplitude,  $v$  is the velocity amplitude and  $\omega$  is the angular frequency. As depicted in Fig. 7 and agreed with the computed mode shape in Fig. 6, four anti-nodes and three nodes are observed along the length of the wedge, with the largest displacement ( $\sim 1.5 \mu\text{m}$  at 0.1 W

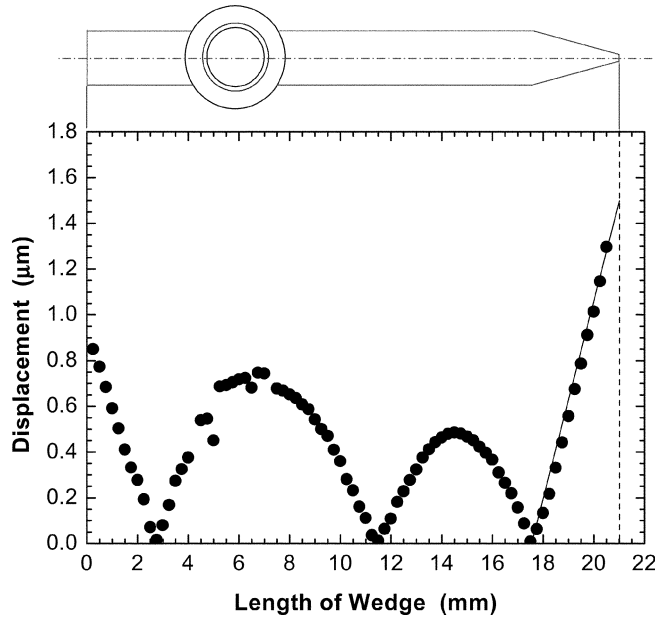


Fig. 7 Measured vibration displacement distribution along the wedge of the *smart* transducer

power) being located at the tip of the wedge, i.e., 21 mm. That is, the wedge is forced to vibrate in the second free-free flexural mode (Graff 1975).

### 3. Process tests

#### 3.1. Impact force detection

The *smart* transducer was installed in an ASM AB510 semiautomatic wedge bonder for performing process tests. For the impact force detection, the ring sensor inside the transducer was connected to a digitizing oscilloscope (Agilent Infiniium 54810A) via a charge amplifier (Kistler 5015A) with a 10 kHz low-pass filter. For comparison, an ASM standard strain gauge force sensor having sensitivity of 543.5 mV/N was also embedded in the workchuck of the bonder underneath the device to be bonded. The output signal of the force sensor was amplified by a signal conditioner (PCB Piezotronics 8120-130A) before being captured simultaneously by the oscilloscope.

Fig. 8 shows the impact signals detected by both the ring and force sensors when the transducer is lowered to apply a bond force of 0.3 N to an ASM standard COB test device (Fig. 1) with and without an aluminum bond wire (~32 μm diameter). In the absence of the bond wire (Fig. 8a), both sensors detect a sharp impact pulse at the moment when the device is hit by the wedge. In more details, when the wedge is traveling downward and touches the device on the surface, the driver of the transducer would experience an upward bending force that compresses the upper part of the ring sensor to produce an impact signal based on the piezoelectric effect. This impact force is also detected by the force sensor situated below the device in addition to the applied static bond force (0.3 N). If the wire is present (in the normal bonding condition) (Fig. 8b), no impact signal is detected by the ring sensor at the time of

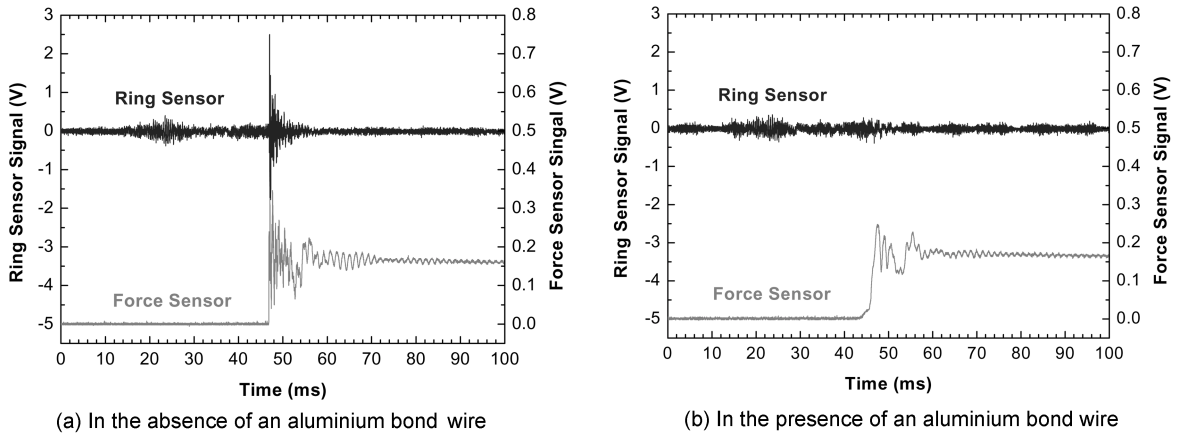


Fig. 8 Impact signals detected by the ring and force sensors

the wedge touchdown. However, the output of the force sensor still rises up even though the rising is gradual and has lower amplitude as compared with the case when the wire is absent. This is because the wire acts as a “passive damper” to absorb the impact energy generated by the downward motion of the wedge. Thus, the impact signals detected by the ring sensor are significantly different in the presence and absence of the bond wire. This implies that the ring sensor is practically viable for in-process missing wire detection by noticing the occurrence of this impact pulse.

### 3.2. Bond quality monitoring

The *smart* transducer in the bonder was used to bond 300 aluminum wires on the ASM standard COB test device (Fig. 1). For each bond point, the transducer was energized using 0.1 W power at its resonance frequency of 62.4 kHz for 20 ms under a bond force of 0.3 N. The vibration signals detected by the ring sensor was concurrently fed into two separated charge amplifiers (Kistler 5015A) operating with a 62.4 kHz band-pass filter and a 124.8 kHz band-pass filter for extracting the fundamental and second harmonic components, respectively. The filtered signals were captured by a digital oscilloscope (Agilent Infiniium 54810A). The quality of each bonded wire was examined by an optical projector (Nikon V-12A) with 200 times magnification for visual inspection and then by a pull tester (Royce Instruments System 550) for a standard pull test. The visual inspection involves visual checking the appearance and deformation ratio of the wire bonds, while the pull test is a destructive test aimed to measure the pull strength of the bonded wires by pulling them at their loop tops vertically until ruptures occur (Or 2001). Hence, the term “good bond” is defined as a bond possessing both higher pull strength and smaller deformation ratio with smaller standard deviations. The most desirable case is breaking at the wire span followed by breaking at the bond neck. For the poor bond, the bond can completely be peeled off from the bonding surface in the pull test. This is attributed to the weak intermetallic adhesion between the wire and the bond pad/lead surface. For the nonstick bond, the wire cannot stick on the bonding surface after the completion of the whole bonding period.

Fig. 9 shows the fundamental and second harmonic signals of a typical good bond. The amplitude of both signals ramps up quickly to their respective maxima in the first 3 ms (6-9 ms) and then shows a rapid drop for the following 7 ms (9-16 ms) before reaching a long low steady-state amplitude (16-26

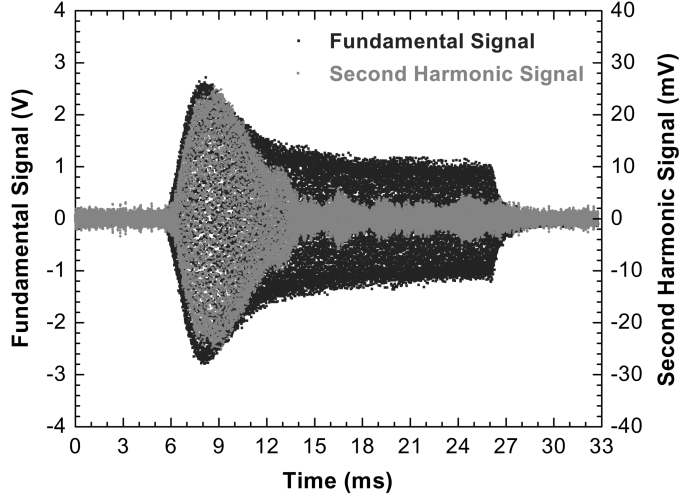


Fig. 9 Fundamental and second harmonic signals captured by the ring sensor during a bonding operation

ms). We have correlated this phenomenon to a qualitative bonding mechanism, which states that the initial high amplitude period promotes maximum surface disruption and area of contact (the cleaning phase), whilst the subsequent lower steady-state amplitude periods promote the formation of individual microwelds (the bonding phase) and permit consolidation of bond strength (the tempering phase). It is postulated that the larger and faster the amplitude drops, the more and faster the energy is used up in the bond formation (Or, *et al.* 1998a, Or 2001). It is also interesting to note that the second harmonic signal exhibits a very characteristic amplitude change in comparison with its fundamental signal counterpart. The observation agrees with those reported previously in that the second harmonic signal is more sensitive to changes in mechanical impedance of the bond zone due to the bond formation (Or, *et al.* 1998, Chan, *et al.* 2001a, Chu, *et al.* 2003).

Alternatively, the observation can be explained by a physical model built using one-dimensional elastic wave theory (Yan 1995). For steady state conditions, the displacement distributions along the length of the piezoelectric driver as shown in Fig. 10 can be expressed in the following forms:

$$0 < z_b < l_b, \quad u_b = a_b \cos k_b z_b \quad (2a)$$

$$0 < z_s < l_s, \quad u_s = a_s \cos k_s z_s + b_s \sin k_s z_s \quad (2b)$$

$$-l_f < z_f < 0, \quad u_f = a_f \cos k_f z_f \quad (2c)$$

where  $a_b$ ,  $a_s$ ,  $b_b$ , and  $a_f$  are arbitrary constants and  $k$  is the wave number. The corresponding stress distributions are:

$$0 < z_b < l_b, \quad T_b = T_b S_b = -Y_b k_b a_b \sin k_b z_b \quad (3a)$$

$$0 < z_s < l_s, \quad T_s = Y_s S_s - \frac{g_{33}^D}{s_{33}^D} D_3 = -Y_s k_s a_s \sin k_s z_s + Y_s k_s b_s \cos k_s z_s - \frac{g_{33}^D}{s_{33}^D} D_3 \quad (3b)$$

$$-l_f < z_f < 0, \quad T_f = Y_f S_f = -Y_f k_f a_f \sin k_f z_f \quad (3c)$$

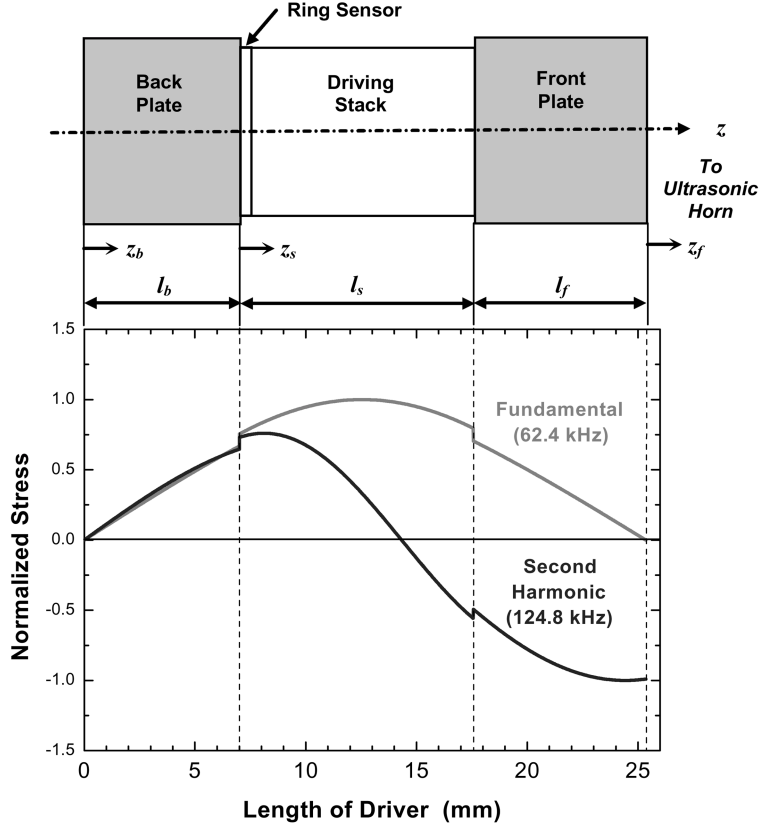


Fig. 10 Calculated stress distributions along the length of the *smart* driver

where  $Y$ ,  $S$ ,  $g_{33}$ ,  $s_{33}^D$  and  $D_3$  are the Young's modulus, axial strain, piezoelectric voltage coefficient, elastic compliance at constant electric displacement and the electric displacement, respectively. The boundary conditions for the displacements and the stresses are as follows:

At the interface of  $z_b=l_b$  and  $z_s=0$ , we have  $u_b(l_b)=u_s(0)$  and  $T_s(l_b)=T_s(0)$ , i.e., the continuity of displacement and stress.

$$a_b \cos k_b l_b = a_s \quad (4a)$$

$$-Y_b k_b a_b \sin k_b l_b = Y_s k_s b_s - \frac{g_{33}^D}{s_{33}^D} D_3 \quad (4b)$$

At the interface of  $z_s=l_s$  and  $z_f=-l_f$ , we have  $u_s(l_s)=u_f(-l_f)$  and  $T_s(l_s)=T_f(-l_f)$ , i.e., the continuity of displacement and stress.

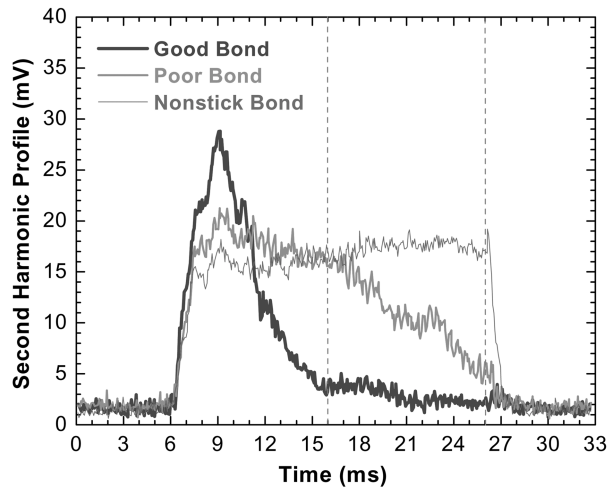
$$a_s \cos k_s l_s + b_b \sin k_s l_s = a_f \cos k_f l_f \quad (5a)$$

$$-Y_s k_s a_s \sin k_s l_s + Y_s k_s b_s \cos k_s l_s - \frac{g_{33}^D}{s_{33}^D} D_3 = Y_f k_f a_f \sin k_f l_f \quad (5b)$$

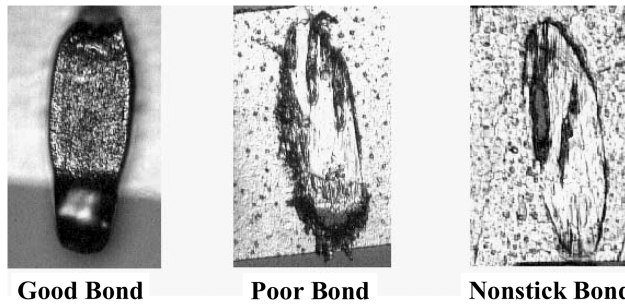
Solving Eqs. (4) and (5),  $a_f$  can be related to  $a_b$  by

$$\frac{a_f}{a_b} = \frac{\frac{Z_b^c A_s}{Z_s^c A_b} \sin k_b l_b + \cos k_b l_b \tan \frac{k_s l_s}{2}}{\frac{Z_f^c A_s}{Z_s^c A_f} \sin k_f l_f + \cos k_f l_f \tan \frac{k_s l_s}{2}} \quad (6)$$

which in turn relates to  $a_s$  and  $b_s$  through Eqs. (4) and (5). Hence, as long as either one of these constants is known, the others can be determined. Then, the displacement and stress distributions along the piezoelectric driver can be found readily from Eqs. (2) and (3), respectively. Fig. 10 shows the stress distributions in the driver when operating at 62.4 kHz and 124.8 kHz. It is seen that the fundamental frequency at 62.4 kHz produces a symmetric stress distribution having 0.5 longitudinal wavelength (the length of driver), whereas the second harmonic at 124.8 kHz gives rise to an asymmetric stress distribution corresponding to  $\sim 0.75$  longitudinal wavelength. This asymmetric stress distribution not only leads to a larger stress-frequency sensitivity (a larger slope) but also results in



(a) Amplitude profiles



(b) The corresponding optical micrographs

Fig. 11 Amplitude profiles of the second harmonic signals for different bond qualities. (a) Amplitude profiles, (b) The corresponding optical micrographs

two stress maxima: one at the interface of driving stack and back plate and one at the front plate. As piezoelectric sensor is sensitive to the changes in applied stress, and by placing the ring sensor at the driving stack-back plate interface, the bond quality can be monitored in-situ by observing changes in the amplitude of the second harmonic signal of the ring sensor.

Fig. 11(a) shows the amplitude profile (envelope) of the second harmonic signals obtained from a good bond, poor bond and nonstick bond, whilst their corresponding optical micrographs are illustrated in Fig. 11(b). The sign of good bonds is that their signal amplitudes generally show an initial distinctive peak and then undergo a significant drop to a very low value after the application of ultrasound for 3 ms and 10 ms, respectively. If their associated bonded wires are pull-tested, wire bonds will remain essentially intact on the bonding surface. Poor bonds also have an initial period of high amplitude, but it is rather low and keeps decreasing gradually without the steady-state amplitude period. This type of wire bonds are often peeled off from the bonding surface after the pull test, resulting in a large portion of unwelded area due to the formation of voids. For the nonstick bonds, the signal amplitude does not drop throughout the whole bonding period; it sometimes increases with increasing time instead. No actual welded areas are observed from their footprints. In short, Fig. 11(a) indicates that good bonds generally have a unique rapid drop in their amplitude profiles to a long low steady-state value after the ultrasound has been turned on for 10 ms. Hence, the area under the signal profiles of the ring sensor after 10 ms (16-26 ms in Fig. 11a) ( $A$ ) was used as an indicator for bond quality monitoring.

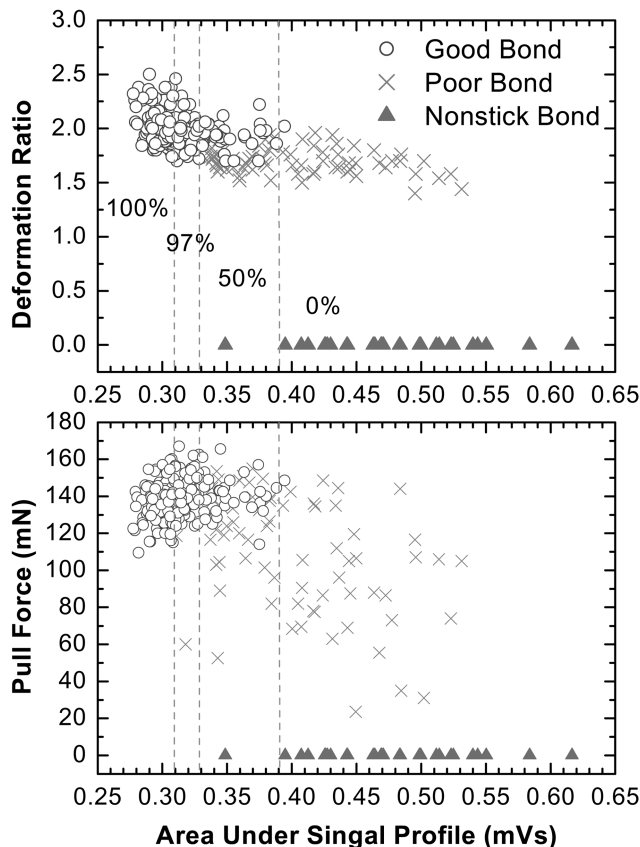


Fig. 12 Deformation ratio and pull force as a function of  $A$

Fig. 12 plots the bond deformation ratio and wire pull force as a function of  $A$ . It is obvious that the majority of good bonds dominate the regions with smaller values of  $A$  ( $<0.33$ ). With increasing  $A$ , the possibility of obtaining poor or nonstick bonds is increased. For  $A < 0.31$ , all bonds are classified as good bond. For  $A < 0.33$ , only 97% are ranked as good. For  $0.33 \leq A \leq 0.39$ , only 50% are good bond. If  $A > 0.39$ , no good bonds are found.

#### 4. Conclusions

A PZT ring sensor having a partially coated silver electrode on its upper segment has been installed in the Langevin driver of a 62 kHz wedge transducer to form a *smart* transducer for in-process monitoring of ultrasonic wedge bonding. This single sensor possesses a dual functional ability of 1) detecting the absence of bond wires by monitoring the presence of impact force signals; and 2) differentiating different bond qualities, such as good bond, poor bond and nonstick bond, by monitoring changes in the amplitude of the second harmonic of ultrasonic vibration signals. This smart transducer has been incorporated into a real-time automatic process control system for wire bonding (Chan, *et al.* 2001b), and bonding process drifting towards unacceptable conditions can be avoided.

#### Acknowledgements

This work was supported by the Centre for Smart Materials of The Hong Kong Polytechnic University, the Innovation and Technology Fund under Grant UIM/29 of the HKSAR Government and ASM Assembly Automation Ltd. Technical support from Mr. Paul Wing Po Chu is also acknowledged.

#### References

- Chan, H. L. W., Chiu, S. S., Or, S. W., Cheung, Y. M., Yuen, C. W. and Liu, P. C. K. (1999), "Sensors for ultrasonic wire bonding process control", *Ferroelectrics*, **232**, 211-216.
- Chan, H. L. W., Chiu, S. S., Or, S. W. and Cheung, Y. M. (2001a), "Piezoelectric sensor for measuring bonding parameters", US Patent, No. 6 279 810 B1.
- Chan, H. L. W., Or, S. W. and Choy, C. L. (2001b), "Ultrasonic transducer", US Patent, No. 6 286 747 B1.
- Charles, K. Jr. (1989), "Electrical interconnections", *Electronic Materials Handbook Volume 1*, ASM International.
- Chiu, S. S., Chan, H. L. W., Or, S. W., Cheung, Y. M. and Liu, P. C. K. (2003), "Effect of electrode pattern on the outputs of piezosensors for wire bonding process control", *Mater. Sci. Eng. B-Solid State Mater. Adv. Technol.*, **99**(1-3), 121-126.
- Chu, P. W. P., Chong, C. P., Chan, H. L. W., Ng, K. M. W. and Liu, P. C. K. (2003), "Placement of piezoelectric ceramic sensors in ultrasonic wire-bonding transducers", *Microelectronic Engineering*, **66**, 750-759.
- Frederick, J. R. (1975), *Ultrasonic Engineering*, John Wiley & Sons, New York.
- Graff, K. F. (1975), *Wave Motion in Elastic Solids*, Clarendon Press, Oxford, UK.
- Harman, G. G. (1997), *Wire Bonding in Microelectronics: Materials, Processes, Reliability, and Yields*, McGraw-Hill, New York.
- Hu, C. M., Guo, N., Du, H. and Xu, L. M. (2003), "Dynamic characteristics of stacked piezoelectric transducers of ultrasonic wire bonders used in integrated circuit packaging", *Proceedings of the Institution of Mechanical Engineers Part C - J. Mech. Eng. Sci.*, **217**(3), 341-352.
- Neppiras, E. A. (1973), "The pre-stressed piezoelectric sandwich transducer", *Proceedings of Ultrasonics*

*International 1973 Conference*, 295-302.

Or, S. W., Chan, H. L. W., Lo, V. C. and Yuen, C. W. (1998a), "Dynamics of an ultrasonic transducer used for wire bonding", *IEEE Trans. Ultrason. Ferroelectr. Freq. Control*, **45**(6), 1453-1460.

Or, S. W., Chan, H. L. W., Lo, V. C. and Yuen, C. W. (1998b), "Ultrasonic wire-bond quality monitoring using piezoelectric sensor", *Sens. Actuator A-Phys.*, **65**, 69-75.

Or, S. W. (2001), "High frequency transducer for ultrasonic bonding", PhD Dissertation, The Hong Kong Polytechnic University.

Pufall, R. (1993), "Automatic process control of wire bonding", *Proceedings of 43<sup>rd</sup> Electronic Components and Technology Conference*, 159-162.

Rodwell, R. and Worrall, D. A. (1985), "Quality control in ultrasonic wire bonding", *Hybrid Circuits*, **7**, 67-72.

Yan, Z. and Lin, Z. (1995), "Optimum design for sandwich transducer - by analyzing effect of structure and material parameters of transducer on its performance", *Acta Acustica*, **20**(1), 18-25.

*JK*